Electrochimica Acta 110 (2013) 437–445

Contents lists available at ScienceDirect

Electrochimica Acta

journal homepage: www.elsevier.com/locate/electacta

Direct spectroscopic monitoring of conductance switching in polythiophene memory devices

Lian C.T. Shoute[a,b], Yiliang Wu[c], Richard L. McCreery[a,b,*]

[a] National Institute for Nanotechnology, 11421 Saskatchewan Dr, Edmonton, Alberta T6G 2M9, Canada
[b] Department of Chemistry, 11227 Saskatchewan Dr, University of Alberta, Edmonton, Alberta T6G 2G2, Canada
[c] Xerox Research Centre of Canada, 2660 Speakman Drive, Mississauga, Ontario L5K 2L1, Canada

ARTICLE INFO

Article history:
Received 24 October 2012
Received in revised form
23 November 2012
Accepted 26 November 2012
Available online 3 December 2012

Keywords:
Molecular electronics
Solid state redox
Polythiophene
Nonvolatile memory

ABSTRACT

A large number of nonvolatile memory devices have been reported with both inorganic and organic components, and many of these involve changes in device resistance between a high conductivity "ON" state and a low conductivity "OFF" state. The mechanism of memory action in many of these devices is uncertain, and may be based on many phenomena, including redox reactions, metal filament formation, charge storage in "floating gates", and redistribution of oxide vacancies. We report here a Raman spectroscopic probe of organic polymer memory devices which permits direct monitoring of the doping state and conductivity of polythiophene in a 3-terminal device. The polymer conductance is controlled by voltage pulses between the source and gate electrodes in FET geometry, while the conductance state is read out by a separate circuit between source and drain. The conductance was directly correlated with the Raman determination of the density of polarons in the polymer film, which was shown to control both the "electroforming" process and the conductance switching in working memory devices. The polymer conductance change requires a redox counter-reaction at the gate electrode, and atmospheric effects on performance indicate that water and oxygen reduction are involved. The observations are consistent with a redox process between the gate and source electrodes which modulates the polaron concentration and source–drain conductivity. This mechanism provides a framework for optimization of the device by changing its composition and geometry, particularly the identity of the redox counter-reaction and control of ion mobility.

1. Introduction

Solid-state nonvolatile memory (NVM) has enabled portable electronics in the form of cell phones, media players, and a large number of additional consumer electronic devices. The dominant technology is "flash" memory based on a floating gate field effect transistor (FET) structure using a thin layer of silicon isolated from a write/erase electrode by silicon oxide. Charge injected into the floating gate modulates the FET conductance, and the high and low conductance states are stable for typically >10 years. In terms of volume, more than 100 billion units of solid state NVM were produced as of 2009, with floating gate "flash" by far the most common [1]. While the density and utility of flash memory have increased dramatically in the past decade, it is much slower than dynamic random access memory (DRAM), requires relatively high voltage to "write" and "erase", and has a limited cycle life (10^3–10^5) due to fatigue of the SiO_2 gate insulator. High economic value and the shortcomings of flash memory have stimulated research into a wide range of alternative NVM devices based on both "2-terminal" or "crossbar" geometry and on "3-terminal" structures resembling an FET but usually with a quite different mechanism. Reviews of inorganic [2,3], organic [4], and polymer [5,6] NVM approaches have appeared recently, but several organic approaches which are relevant to the current paper are noted here.

As shown in Fig. 1a, a 2-terminal cross-bar architecture consists of an organic or polymer (O) layer of different thicknesses sandwiched between two conducting electrodes (M) made of identical (MOM) [7–10] or different materials (MOM′) [11–13]. When a ferroelectric polymer is used as the organic layer, bias induced switching between two stable polarization states can form the basis for memory [14,15]. In non-ferroelectric polymers, the organic layer can also be impregnated with metal nanoparticles [16,17], to impart or enhance the desired memory response. Conductivity switching has been reported in many cross-bar devices fabricated from a wide variety of organic molecules and polymers with and without additional stacking layers. These devices often require an initial

* Corresponding author at: Department of Chemistry, 11227 Saskatchewan Dr, University of Alberta, Edmonton, Alberta T6G 2G2, Canada. Tel.: +1 11 780 641 1760.
E-mail addresses: mccreery@ualberta.ca, richard.mccreery@ualberta.ca (R.L. McCreery).

0013-4686/$ – see front matter © 2012 Elsevier Ltd. All rights reserved.
http://dx.doi.org/10.1016/j.electacta.2012.11.111

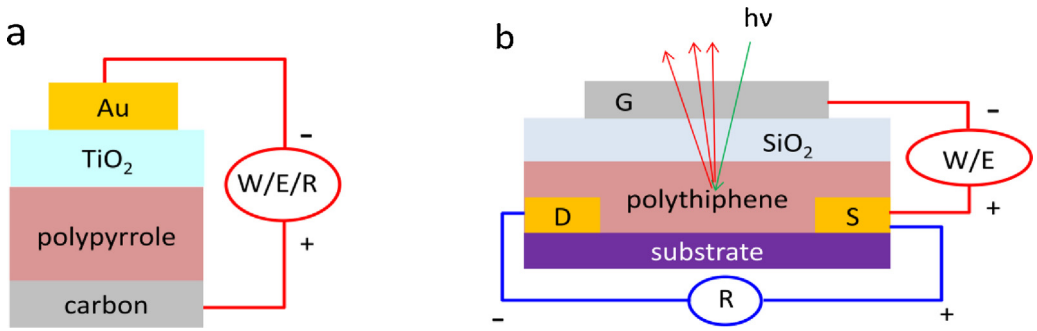

Fig. 1. Schematics of 2-terminal cross bar (a) and three-terminal (b) memory devices. Figure b also shows Raman probe of the channel through Pt gate.

"electroforming" step to jumpstart the device, where a high voltage is applied to initiate conductance switching [5,6]. The device can then be subsequently operated at lower voltages. Although the mechanism of conductivity switching in these devices has often been attributed to the intrinsic properties of the stacked layer materials, clear determinations of switching mechanism are rare [4], and in many cases the data can be explained by filament formation and destruction [11,18–20].

Three-terminal NVM devices with geometries similar to that of field effect transistors (FET) have two potential advantages over the 2-terminal devices. First, the FET geometry is already widely used in both processors and flash memory, so integration of a new 3-terminal NVM device with existing manufacturing should be possible without drastic processing changes. Second, the "write/erase" (W/E) circuit, often between the "gate" and "source" shown in Fig. 1b can be separated from the "read" circuit between the "source" and "drain". As will be discussed later, this separation permits nondestructive readout, independent control of W/E and read events, and allows direct correlation of the conductance readout with the redox properties of the organic or polymeric semiconductor.

Existing three-terminal organic nonvolatile memory (ONVM) devices can be classified into three categories based on the mechanisms of operation, namely ferroelectric (FeFET), charge trap (CtFET), and floating gate OFET (FgFET) memory. In FeFET memory, ferroelectric polymers which have large intrinsic dipole moments are used as the gate dielectric. Reorientation of the dipole by a "write" voltage results in a persistent change in the channel (S-D) conductance. The conductive state is retained even when the power is turned off due to remanent polarization. Application of "erase" bias reverses the dipoles and returns the device to the low conducting state [6,14,21–23]. In CtFET memory [24–27], a polymer layer called an 'electret' is added between the gate dielectric and the organic semiconductor (OSC) layers. For example, in CtFET with p-type OSC, the carriers accumulated in the channel upon application of $-\Delta V_G$ can tunnel and get trapped in the electret layer. The positive trapped charges screen the gate field and shifts threshold voltage (ΔV_{th}) to a more negative value. ΔV_{th} is the gate voltage at which the carrier accumulation is high enough to make the channel conducting. The trapped charges in the electrets can be detrapped by application of the reverse $+\Delta V_G$, shifting ΔV_{th} to its initial value. Hence, ΔV_{th} of the device can be reversibly shifted between these two ΔV_{th} values, thereby yielding a high ON and low OFF channel currents at a particular ΔV_G, preferably at $\Delta V_G = 0$ V. The difference in the ΔV_{th}, obtained on applications of $\pm\Delta V_G$, is the memory window and is proportional to the trapped charge density in the electrets. The mechanism of operation of floating gate OFET (FgFET) [28–30] memory is similar to CtFET except that the charge trapping sites in this case are made of metal or semiconducting nanoparticles or conjugated organic molecules either embedded in gate dielectric or sandwiched between two different polymer layers constituting blocking and tunnel layers. Some OFET devices exhibit a persistent "threshold voltage shift" or "bias stress effect" which is associated with device degradation [25,31–33]. Although the voltage shift is often attributed to trapped charge, the location of that charge and the mechanism underlying the memory effect are not yet clear [31]. Our group has reported 2-terminal low-volatility memory devices based on redox reactions in small organic molecules [34,35], TiO_2 [36–38], and conducting polymers [39–41]. We used in situ Raman and UV–Vis spectroscopy to monitor structural changes in finished devices, in order to correlate conductivity and memory effects to chemical structure. Spectroscopy of polythiophene devices showed that voltage pulses resulted in reversible oxidation of the polymer to its conducting "polaron" state, and that the process required a corresponding reduction reaction to accompany polymer oxidation. We determined that residual water in a polythiophene/oxide "stack" and a catalytically active electrode are required for long retention of the polaron state of the polymer. Investigation of a variety of device compositions containing different metal oxides and various electrode materials indicated that the catalytic reduction of H_2O to chemisorbed hydrogen and mobile hydroxide ion was the most likely counter-reaction for polymer oxidation [39]. However, the oxide layer in the 2-terminal geometry prevented direct correlation of spectroscopic results with device conductance, since the oxide itself had low conductivity. Furthermore, when the oxide is thin enough to permit electrical observation of polymer conductance changes, recombination reactions are likely which decrease retention time. In order to establish that polymer oxidation is directly responsible for observed conductance changes, we adopted the 3-terminal geometry of Fig. 1b. Not only did the approach permit determination of the conductance switching mechanism, it also revealed useful information about how to control several aspects of memory function by variation of device composition.

2. Experimental

Three terminal organic nonvolatile memory (ONVM) was fabricated on thermally oxidized (~300 nm SiO_2) Si wafer in a bottom contact and top gate geometry. Although "source", "drain", and "gate" labels are used in the 3-terminal devices by analogy to standard FETs, it should be noted that the operation and principles of ONVM differ fundamentally from conventional FETs. Standard photolithographic and lift off techniques were used to pattern the Au (with 5 nm Cr adhesion layer) source and drain electrodes on the wafer. The wafer was then diced into 13 mm × 18 mm sized chips with each chip having four source and drain pairs. Each source–drain pair has the same channel width of 500 μm and the channel length was varied from 2 to 100 μm. After liftoff of the residual photoresist with acetone (Fisher HPLC), the chip was ultrasonicated with baths of acetone, Millipore water, and 2-propanol (Fisher HPLC) in sequence, and dried with a stream of N_2. Electronic grade regioregular polythiophene, either 0.8 wt%

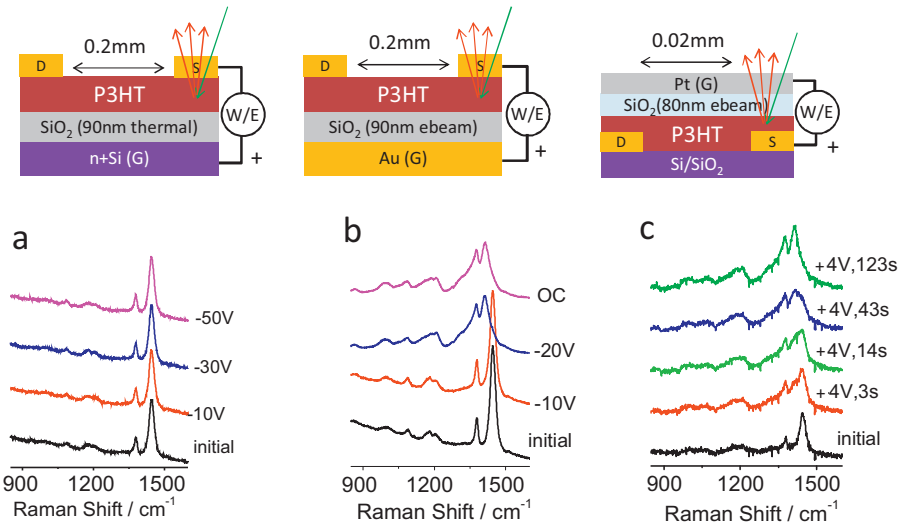

Fig. 2. Schematics illustrating the device structures, compositions, and the locations of the Raman probe (top panel). Raman spectra of P3HT were obtained by excitation with 780 nm by probing through the source: (a) bottom gate-top contact OFET with thermally grown SiO_2 (90 nm) on n + Si as gate; (b) bottom gate-top contact OFET with ebeam SiO_2 (90 nm) deposited on Au as gate; and (c) top gate-bottom contact OFET with Pt as gate and ebeam SiO_2 (80 nm) gate dielectric deposited on P3HT. Probing the channel region yields a similar spectrum to that of the source for each structure (not shown).

poly-3-hexylthiophene (16k MW, Ricke Metal Inc.) or 0.3 wt% poly-3,3-didodecylquaterthiophene (6k MW, Xerox Ltd.) in 1,2-dichlorobenzene was spin coated at 1000 rpm for 120 min on the cleaned chips as described earlier to yield polythiophene layer thickness of 20–50 nm. The sample was then dried at 90 °C for 1 h and annealed at 120 °C for 10 min in vacuum (~10^{-2} Torr) as described earlier [39,42,43]. Gate dielectric SiO_2 (99.9% Kurt J. Lesker) and the Pt (99.9% Kurt J. Lesker) gate electrode were deposited at ~10^5 Torr base pressure through appropriate shadow masks by ebeam evaporation (Kurt J. Lesker PVD75) at the rate of 1.0 and 0.2 Å/s respectively to complete the device fabrication.

The performance of the ONVM devices was characterized under either ambient or portable controlled environment chamber using a custom built electronic characterization setup consisting of National Instruments 6111 or 6120 DAQ board controlled by Labview software to execute voltage sweeps and record the resulting current after amplification by an SRS 570 current amplifier. Thermo/Nicolet Raman microscope with a CCD detector operating at 780 nm was used to probe the source, drain, and the channel of ONVM device which has a channel length of 20 μm. Spectra recordings were carried out with 10× magnification at a typical CCD detector integration time of 2–10 s as described earlier. A Gamry reference 600 potentiostat operating on PHE 200 physical electrochemistry software was used to run chronoamperometry software to apply write/erase pulses, and cyclic voltammetry software to read the channel current during the in situ Raman experiment. Electrical and in situ Raman experiments under controlled atmosphere were carried out in a portable custom fabricated chamber with quartz window for Raman spectroscopic measurements and inlet and outlet for purging gas. Relative humidity in the chamber was controlled by mixing dry N_2 or O_2 (PRAXAIR > 99.99%) with moisture saturated N_2 or O_2 obtained by purging into Millipore water in an enclosed glass cylinder. Relative humidity in the chamber can be controlled to any desired value by mixing dry and wet gas in appropriate proportion.

Redox based ONVM memory presented here is based on top gate, bottom contact geometry with P3HT as the OSC as shown in Fig. 1b. The bottom contacts consisting of the source and the drain electrodes were photolithographically patterned on a 13 mm × 18 nm Si chip with 300 nm thermal SiO_2. 80 nm SiO_2 gate dielectric and 9 nm Pt gate electrode were ebeam deposited (~1×10^{-5} Torr base pressure) on top of ~40 nm P3HT using appropriate shadow masks. The width of the SiO_2 gate dielectric was significantly larger than the top Pt gate to avoid edge effects. The Pt gate spans the channel and overlaps with a 500 μm portion of both the source and drain electrodes to facilitate capacitive electrochemical charging. The channel width was fixed at 500 μm and the channel length was varied from 2 to 100 μm. According to IUPAC convention, potential differences between electrodes are noted as "Δ*V*", e.g. "ΔV_{SG} = +2 V" indicates 2 volts between the S and G electrodes, with S positive.

3. Results

Fig. 2 shows Raman spectra obtained during operation of 3-terminal structures with three different configurations containing P3HT and SiO_2. The Raman probe was positioned over the source (S) and spectra were acquired before and during the application of a bias voltage between the S and G electrodes. The spectra labeled "initial" were obtained before any bias was applied, and correspond to the Raman spectrum of undoped P3HT reported previously [39]. For the case of a 90 nm thick thermal SiO_2 dielectric layer (Fig. 2a), no changes in the Raman spectrum were observed when the n + Si gate was biased up to −50 V, with more negative bias causing breakdown. A positive bias to the n + Si gate also had no observable effect on the Raman spectrum. Fig. 2a represents a standard OFET configuration, in which positively charged carriers should be generated in the P3HT by the negative gate bias. However, the carrier density is apparently too low to detect by Raman spectroscopy in this configuration, due to the small capacitance (~40 nF) of the device. Fig. 2b shows a quite different result for a modified configuration in which the n + Si gate is replaced with Au, and the gate dielectric is a 90 nm layer of e-beam deposited SiO_2. Not only does the Raman spectrum change with a negative gate bias to that of the P3HT polaron [39], but this change persists after the bias is removed. The Raman spectra of P3HT neutral and polaron obtained here are similar to those obtained in solution before and after oxidation with $FeCl_3$ (supporting information Figure S1) respectively. As reported for a 2-terminal analog of the structure shown in Fig. 2b, the catalytic Au surface and disordered SiO_2 create an electrochemical cell in which P3HT is oxidized and residual H_2O is reduced, accompanied by ion transport through the porous SiO_2 film [39]. The polaron was

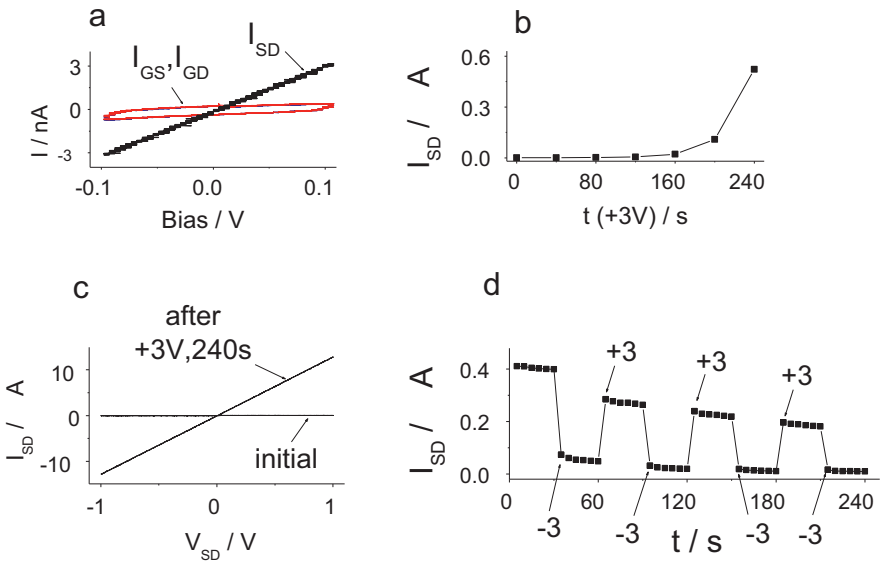

Fig. 3. Electrical characteristics of a P3HT ONVM device in O_2 atmosphere at RH of 31%: (a) *I–V* scans (scan rate of 0.01 V/s) of pristine as fabricated P3HT based ONVM device; (b) device activation, I_{SD} versus *t*, *t* is the duration of +3 V ΔV_{SG} application; (c) a typical *I–V* scans before and after device activation; (d) variation in I_{SD} for alternating −3 and +3 V ΔV_{SG} pulses. V_{SD} for read pulses was +0.1 V.

formed in the channel as well as between the source and gate, as indicated by Raman spectra obtained when the Raman probe was either on the source or displaced ~10 μm from the source electrode in the channel. Fig. 2c shows a 3-terminal structure more amenable to patterning and fabrication, using Pt instead of Au for the gate to avoid enhanced Raman scattering at the Au/P3HT interface. The neutral P3HT spectrum observed in both the channel and on the source gradually changes to that of the polaron when the source is biased at +4 V relative to the gate electrode. The configuration shown in Fig. 2c was used for all subsequent experiments, unless noted otherwise below. Note that the stack order is reversed between Fig. 2b and c, but the polythiophene is oxidized in both cases when the adjacent contact is biased positive.

The transition from neutral to polaron spectrum apparent in Fig. 2c was correlated with the conductance between the source and drain electrodes during simultaneous monitoring of the Raman spectral changes. Fig. 3a shows the current–voltage (*I–V*) response for all three combinations of two electrodes, for the as-fabricated device in ambient air. As expected for undoped P3HT, the currents are small, with similar response for the S-G and G-D circuits and an S-D resistance of ~33 MΩ. The S-G and G-D responses show a capacitive component due to the expected parallel-plate capacitance between the S and D electrodes and the gate electrode. The S-D response shows higher conductivity than S-G, but both are quite small due to the low doping level of the initial P3HT layer.

The initial device was tested for memory behavior by applying $\pm\Delta V_{SG}$ pulses (between S and G electrodes) in ambient air, intended to oxidize and reduce the polythiophene to its conducting and non-conducting forms, respectively. As shown in Figure S2, such pulses caused small but reproducible changes in the S-D conductance, with a ratio of high/low S-D conductance <2 and currents below 0.1 μA. Repeated application of W/E pulses increased the ON/OFF to ~15, but the S-D currents remained small, <1 μA at $\Delta V_{SD} = \pm 0.1$ V. After some trial and error, we found that the S-D conductance and ON/OFF ratio could be increased significantly by intentionally generating polarons in the polymer layer with repeated +3 V pulses between the S and G electrodes, with G biased negative. This "activation" process was sensitive to humidity and ambient oxygen (see below), so these conditions were controlled at 31% relative humidity (RH) in an oxygen atmosphere. Fig. 3 shows the S-D current during a series of +3 V ΔV_{SG} pulses (Fig. 3b) and the resulting *I–V* curve between S and D (Fig. 3c) after activation compared to the initial value. After this activation process, I_{SD} increased by a factor of >500, implying that a higher concentration of the conducting "polaron" form of P3HT is formed during activation. Application of a sequence of −3 V, 2 s and +3 V, 2 s pulses caused repeatable changes in the S-D current (Fig. 3d), with the conductance changing by a factor of 6–8. The oscillation of I_{SD} shown in Fig. 3d was repeatable for at least 60 complete R/W/R/E cycles, with no obvious degradation of response. It is important to note that the gate–source and gate–drain *I–V* curves maintained the capacitive and low conductance (~1 nA) states shown in Fig. 3a after activation, conductivity switching, and retention measurements. W/E pulses shorter than 1 s produced smaller changes in device conductance, with a 100 ms W pulse changing channel conductance by approximately a factor of 10. The reason for the slow response is under investigation, but is likely due to ion transport time in the solid state memory cell.

In order to determine structural changes in the semiconducting P3HT layer of the memory devices during the activation and switching shown in Fig. 3, Raman spectra and *I–V* curves of a working device were obtained immediately after application of source–gate pulses. As indicated in Fig. 2, a Raman microscope was positioned to obtain spectra through the partially transparent Pt gate, above the source, drain, or channel regions. The initial Raman spectra at the S and D electrodes or in the channel are indistinguishable from those of the unbiased device shown in Fig. 2c, and correspond to the reference spectrum of neutral P3HT (Figure S1). Fig. 4a shows the S-D current (at $\Delta V_{SD} = +0.1$ V) during an activation similar to that shown in Fig. 3b. The spectrum of the pristine device with $I_{SD} = 3.2$ nA (at $\Delta V_{SD} = +0.1$ V) has P3HT predominantly in the neutral form as indicated by the Raman spectra of the source, channel, and drain. The Raman spectra acquired at different times after the application of +4 V ΔV_{SG} show a decrease in neutral contribution and concomitant increase in polaron contribution to the spectrum. In addition, the polaron/neutral ratio increases faster in the source electrode compared to the channel and the drain. This is expected as the activation voltage pulse is applied between the S and G electrodes. The appearance of the polaron spectrum at the drain electrode implies that oxidation of P3HT propagates across the channel and onto

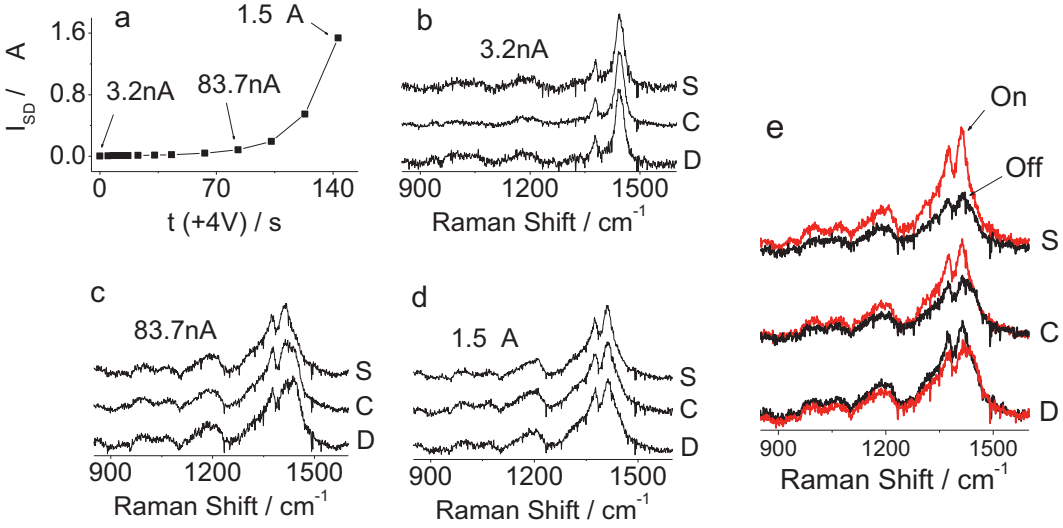

Fig. 4. In situ Raman spectra (780 nm excitation) and electrical measurements of a P3HT based ONVM device under ambient condition: (a) I_{SD} versus t plot of the device activation with +4 V ΔV_{SG}; (b) Raman spectra probing the source (S), channel (C), and drain (D) of the pristine device before activation; (c, d) representative Raman spectra probing the source, channel, and drain measured immediately after application of +4 V ΔV_{SG} pulse of durations (c) after 83 s, and (d) after 143 s. (e) Raman spectra of the activated device after application of W and E ΔV_{SG} pulses of +5 V, 1 s and −5 V, 1 s, respectively.

the drain, despite the fact that the drain electrode is electrically floating during the +4 V pulse. At I_{SD} = 1.5 μA (ΔV_{SD} = +0.1 V), the P3HT spectrum is predominantly that of the polaron. Fig. 4e shows Raman spectral changes which accompany conductance switching, acquired after application of +5 V, 1 s "write" and −5 V, 1 s "erase" pulses. The I–V scan of the S-D gave an ON/OFF ratio of 17.9. Clearly, the Raman spectral changes show that there is a direct correlation between conductivity switching and the P3HT neutral and polaron concentrations. The reasons for the unexpected spectral changes at the floating D electrode are considered below.

To more quantitatively determine structural changes in ONVM devices during the activation and switching shown in Fig. 3, Raman spectra of a working device were obtained simultaneously with gate pulses and I–V curves. As indicated in Fig. 2c, a Raman microscope was positioned to obtain spectra through the partially transparent Pt gate, above the channel region. Fig. 5a shows the SD current (ΔV_{SD} = +0.1 V) during an activation and switching sequence similar to that shown in Fig. 3b and d. Figure S3 shows a series of 20 spectra obtained at the same time as the points of Fig. 5a, for the Raman microprobe positioned over the channel. Although the change from the neutral to polaron spectrum is apparent in the sequence of spectra during activation, more quantitative information from the series can be obtained by rigorous analysis using multivariate curve resolution (MCR), as implemented in Matlab using PLS Toolbox (Eigenvector Research). MCR determines how many components are necessary to account for the spectral variation across the series, and the time course of each component. The only constraints on the analysis imposed by the operator are that the spectra have no negative intensities and the components have no negative contributions. For the data set of Figure S3, two components account for 99.9% of the variance, and their spectra are shown in Fig. 5b. These spectra were determined solely from the spectra of the working memory device, and they match reference spectra for neutral P3HT and its polaron obtained in solution (Fig. 5d).

The contributions of each component to the device Raman spectrum are shown in Fig. 5c, on the same time scale as the I_{SD} plot in Fig. 5a. Clearly the spectral contribution of the polaron tracks the conductance of the channel, providing direct evidence that "activation" consists of electrochemical conversion of neutral P3HT to its conducting form. Furthermore, modulation of the polaron and neutral concentrations by +3 and −3 V source–gate pulses underlies "switching" of the channel conductance during memory cycles. Although the relative concentrations corresponding to the spectral changes indicated in Fig. 5c depend on the relative Raman cross sections for the polaron and neutral P3HT species, it is clear that the polaron contribution is modulated ~30% by the "write" and "erase" ΔV_{SG} pulses.

As noted in the introduction, the main objective of spectroscopic monitoring of the polythiophene memory device is determination of "activation" and "switching" mechanisms, in order to permit device optimization. In the previous section we established a direct correlation between channel conductivity and polaron concentration in the channel of ONVM device. The question now arises about what stabilizes the polarons to maintain conductivity even after the applied ΔV_{SG} has been removed. In a conventional electrochemical cell, a redox counter-reaction and mobile ions maintain electroneutrality and prevent buildup of space charge. In our previous in situ Raman study on cross-bar devices we showed that polaron formation is sensitive to humidity, and stable polarons are formed only in the case of devices which have a Au/SiO_2 or Pt/SiO_2 interface at the counter-electrode, implying that catalytic reduction of water is involved as the redox counter-reaction [39]. In order to determine the species involved in the reduction reaction at the Pt/SiO_2 interface we have examined activation and conductivity switching of Au/P3HT/SiO_2/Pt ONVM devices under controlled conditions as follows: dry N_2 at relative humidity (RH) of ~0%, dry O_2 at RH = 0%, N_2 + H_2O at RH = 28%, and O_2 + H_2O at RH = 30%.

Fig. 6a shows activation of as-fabricated P3HT devices maintained in the four different atmospheres, using the same voltage sequence in each case. For the device in a dry N_2 atmosphere, negligible change in channel conductivity (I_{SD} < 2 nA) was observed even after application +3 V ΔV_{SG} for 370 s. Furthermore, no conductance switching was observed with ±3 V gate pulses for either dry O_2 or dry N_2 (Figure S4). Similarly, for the devices exposed to dry O_2 atmosphere only slight increase in I_{SD}, from 1.9 nA to 6.0 nA, was observed after application of +3 V ΔV_{SG} for 740 s. For a fresh device in an atmosphere of 28% RH in N_2, I_{SD} during activation increased slowly, but remained significantly below that in O_2 (RH = 34%) even after much longer activation time (Fig. 6a). Activation in 34% RH O_2 with the same parameters yields the increase in I_{SD} shown earlier (Figs. 3–5), indicating that both O_2 and H_2O are required for activation. Exposure of devices to acetonitrile vapor as an alternative

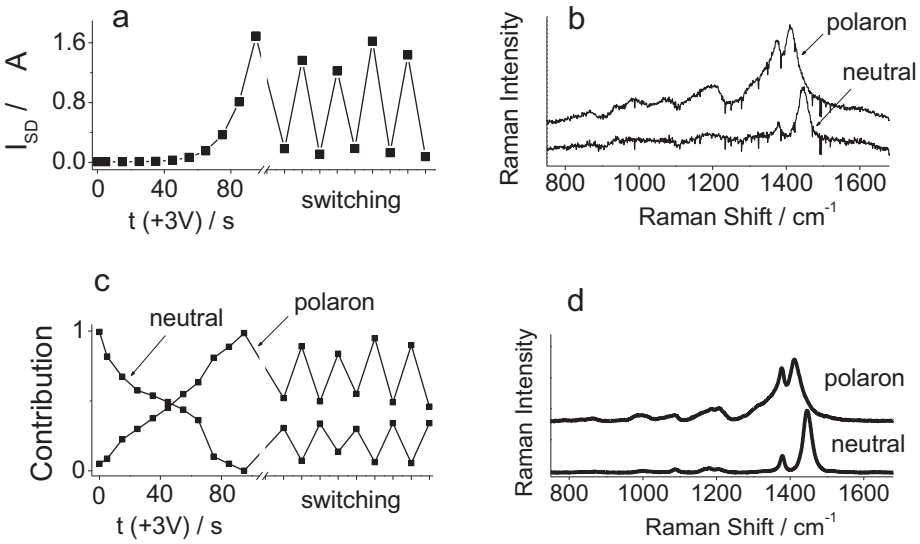

Fig. 5. In situ Raman of a memory device under O_2 atmosphere at RH of 37%: (a) device activation (+3 V ΔV_{SG}) and conductivity switching (±3 V, 1 s ΔV_{SG} pulse); (b) spectra of the two components that account for 99.9% of the variance obtained from multivariate curve resolution (MCR) analysis of a sequence of 20 Raman spectra (780 nm) of the channel recorded after application of SG voltage pulses of different durations; (d) reference Raman spectra P3HT for the neutral from solid thin film and the polaron in $CHCl_3$ obtained by $FeCl_3$ oxidation.

polar molecule in the absence of water vapor prevented activation or switching with or without O_2 present, confirming that water is a reactant in memory operation (see Figure S5). Furthermore, the memory action apparent in Fig. 3d is unstable in N_2 at 28% RH, with a rapid decrease in the ON current with successive cycles (Figure S4d). Once a P3HT device is activated in O_2 with RH ~30%, it may be cycled for many W/R/E/R cycles if maintained in the same atmosphere, as shown in Fig. 7. After an initial decrease in the ON current during the first 3 cycles, the ON and OFF currents showed no further trends with repeated cycling until device breakdown. For the two cases shown in Fig. 7, breakdown occurred after 16 and 27 complete cycles, with greatly reduced ON/OFF ratio observed after breakdown. Device breakdown occurs when the S-G current abruptly increases to a high value of $>10^{-7}$ A (at ΔV_{SG} = +0.1 V) upon application of either W or E pulse. After the breakdown, the device can no longer be switched ON or OFF as shown in Fig. 7.

The device endurance should be affected by several factors, such as the thickness of the SiO_2 and P3HT layers, the roughness of the e-beam deposited source, drain, and gate electrodes, and the relative humidity. The device endurance increases with increasing SiO_2 thickness, and devices in high humidity (>60%) break down during activation.

In order to rule out the possible contributions of other physical phenomena to the observed bistability, such as filament formation, we have investigated several ONVM devices with and without P3HT. A Au/SiO_2/Pt device containing 80 nm of SiO_2 but no P3HT showed no effect of "activation" with ΔV_{SG} = +3 V pulses for several minutes, with no observable increase in channel conductivity. Similar behavior was observed when polystyrene replaced P3HT in the device, and in Au/P3HT/SiO_2 devices with carbon as gate electrode instead of Pt. As noted previously, P3HT polarons could be generated with carbon as gate electrode, but the polarons rapidly revert back to the neutral form when the bias was removed [39].

Finally, a different polythiophene, poly(3,3‴-didodecylquaterthiophene) (PQT) was examined to test the effect of OSC on device characteristics. PQT was chosen because it has attractive processing properties, better stability under ambient conditions, and excellent device characteristics in conventional OFETs [42,43]. Compared to P3HT devices, ONVM devices based on PQT have higher ON/OFF ratio, longer retention, and operate at lower RH, as shown in Fig. 8, indicating that the ONVM characteristics can be modified by the properties of the polymer.

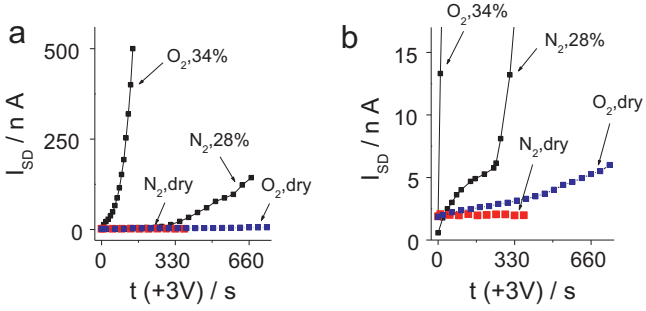

Fig. 6. Activation sequence for four as-fabricated P3HT ONVM devices in various atmospheres, with the time the devices were biased with ΔV_{SG} = +3 V indicated as the *X*-axis. After each ΔV_{SG} bias pulse, the SD current (I_{SD}) was measured at ΔV_{SD} = +0.1 V with ΔV_{SG} at open circuit. Panel (a) shows the SD current for dry O_2, dry N_2, and O_2 with relative humidity of 34%, and N_2 with RH = 28%. Panel (b) is an expansion of the same results along the I_{SD} axis.

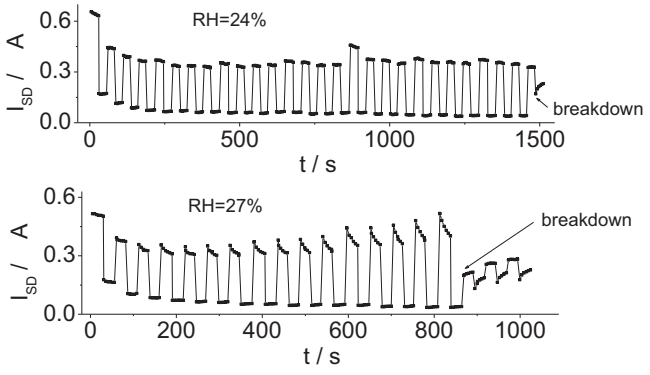

Fig. 7. Endurance tests for P3HT based ONVM devices in O_2 atmosphere at RH of 24% (top panel), and 27% (bottom panel). The devices were activated (by +3 V ΔV_{SG} pulses) to I_{SD} of 0.6–0.7 μA, and subsequently switched with write and erase ΔV_{SG} pulses of +3 V, 2 s and −3 V, 2 s, respectively. Also shown is the device breakdown when the S-G current abruptly increased to $>10^{-7}$ A on application of (a) −3 V, 2 s, and (b) +3 V, 2 s ΔV_{SG} pulses.

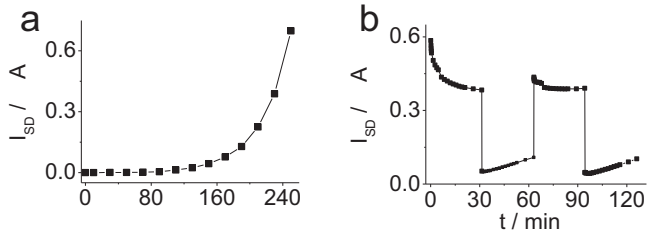

Fig. 8. Device characteristics of PQT based ONVM at RH of 11%: (a) activation with a sequence of +3 V ΔV_{SG}, and (b) switching with W/E pulse of ±3 V, 2 s ΔV_{SG}.

PQT devices exhibit higher sensitivity to the presence of moisture than P3HT devices. At RH >30% where P3HT devices normally operate, the ON states of PQT devices decay quickly and the devices break down on application of a few W/E pulses. More detailed comparison of the devices characteristics of P3HT and PQT based ONVM devices are shown in the supporting information Figure S6.

4. Discussion

The properties of thermal and e-beam SiO_2 play a crucial role in determining device characteristics of OFET and ONVM devices because the former is dense and crystalline, and the latter is porous due to its formation conditions. Since a conventional OFET works via the accumulation of mobile carriers in the channel due to capacitance across the gate dielectric layer, the ordered structure of thermal SiO_2 provides a low-leakage dielectric, and minimizes the possibility of electrochemical reactions induced by the SG bias voltage. In contrast, e-beam SiO_2 is disordered and hygroscopic, and is expected to be more permeable to ions than thermal SiO_2. The ability of porous SiO_2 to transport ions, most likely OH^-, facilitates electrochemical redox reactions and provides counterions for the P3HT polarons, thus compensating the space charge and resulting in a relatively stable ON state. While electrochemical reactions are generally avoided in OFET designs due to the degradation of performance they induce, they play a critical role in the current ONVM devices, since reversible oxidation and reduction of polythiophene results in the high and low conducting states of the devices corresponding to the ON and OFF states, respectively. Many different types of NVM devices based on conductivity switching have been reported in literature which have organic or inorganic or both materials as components in the device structure. These devices, in their pristine as fabricated states, normally do not exhibit electrical bistability under normal operating conditions. Electrical bistability can be induced in these devices by a process that involves an "electroforming" step in which the device is biased until a "soft breakdown" occurs, presumably forming a conducting path which then can be switched ON and OFF electrically [2–4]. In the ONVM device reported here, simultaneous measurements of the electrical characteristics and Raman spectra of the P3HT/SiO_2 ONVM device during "activation" (Figs. 4 and 5) clearly indicate "electroforming" in this case involves oxidation of neutral P3HT to its polaron, with accompanying increase of the channel conductivity. Since the neutral P3HT in the as-fabricated device has low conductivity, the SD current is small, and does not change significantly on application of $\pm\Delta V_{SG}$ pulses. Oxidation of P3HT during activation increases the doping level until "percolation" occurs, i.e. a conducting path is formed between the S and D electrodes. Once formed, this path can be broken and re-made by SG bias pulses. The correlation between SD conductivity and the gain and loss of polaron concentration indicated by the Raman spectrum is a convincing indication that polaron modulation is responsible for ΔV_{SG}-induced conductivity changes. It should be noted that a variety of mechanisms have been proposed for memory effects in FET structures, including filament formation, trapped charge, and redox phenomena [2–4,31–33], but assignment of mechanism is rarely unambiguous. For the case of the polythiophene/silica devices studied here, the spectroscopy provides direct evidence that polaron formation is responsible for the conductance change.

The strong dependence of activation and switching on the presence of O_2 and H_2O indicates that both are likely involved in the redox counter-reaction accompanying polythiophene oxidation. Without such a counter-reaction, the polymer oxidation would be "electrostatic", and would revert to the neutral polymer as soon as the ΔV_{SG} bias is removed. The existence of bistable ON and OFF states indicates that the counter reaction not only accepts electrons removed from polythiophene, but also provides anions (most likely OH^- ions) to compensate the space charge in the polymer generated by polaron formation. Furthermore, the fact that a Pt or Au gate electrode is required implies an electrocatalytic reaction, not present when other electrode materials (e.g. carbon), are used for the gate electrode [39]. The reductions of O_2 and/or H_2O at a Pt surface are quite complex since they involve several steps, and many products are possible, including O_2^-, H_2O_2, OH^-, and H_2. The product distribution is strongly dependent on conditions, and difficult to predict in the solid state devices studied here. However, plausible electrochemical reactions for the Au/P3HT/SiO_2/Pt devices are as follows

Anodic reaction at Au source electrode:

$$P3HT \rightarrow P3HT^+ + e^-$$

Cathodic reaction at Pt gate electrode:

$$O_2 + 2H_2O + 4e^- \rightarrow 4OH^-$$

Reduction of O_2 all the way to OH^- in a single step is an ideal case, but all mechanisms for O_2 reduction generate OH^- [44–46]. The reductions of O_2 and/or H_2O are slow kinetically, hence the importance of a catalytic surface. The slow kinetics of these counter-reactions is at least part of the reason for the slow switching speed, as well as a possible reason for device breakdown. A recent report by Sharma et al. [33] proposed that proton generation and migration in silica was responsible for the slow degradation observed in OFET performance, and H^+ could be involved in the current devices. Slow electrochemical reactions may lead to side reactions which damage the polymer or other components of the device, possibly including H_2 production which could form gas bubbles. We are currently investigating alternative redox counter-reactions to avoid the dependence on water and oxygen. We reported recently that including a viologen electron acceptor to complement the polymer oxidation eliminated the dependence of the memory effect on water or silica, and produced devices with significantly longer cycle life [47].

Finally, we should comment on the differences between the redox reactions and polaron formation in the current devices and the "bias stress effect" reported in OFETs, since the SiO_2/polythiophene devices have similar structure (Fig. 2a and b). The bias stress effect causes the threshold voltage (ΔV_{th}) of OFETs to shift in the direction of the applied gate voltage with prolonged gate bias [31–33,48–53], and is a significant impediment to applications of OFETs [32]. For example, Sharma et al. reported a shift in threshold voltage of ~15 V in triarylamine OFETs following prolonged gate bias of −20 V for 100 h [33]. Many different mechanisms have been proposed to explain bias stress effect in OFETs, including carrier immobilation due to charge trapping in the OSC or OSC/dielectric interface [48–50,52], bipolaron formation [53], contact degradation [51], and hole assisted proton formation and migration into gate dielectric. Detailed studies by de Leeuw et al. [31–33] showed that hole assisted proton formation and migration into the gate dielectric is the most plausible

mechanism for the bias stress effect. While "bias stress" could involve polaron formation and subsequent immobilization of carriers by trapping, the redox-based memory effect reported here exhibits important differences. The polaron formed in the devices reported here increases conductivity in contrast to the trapped charges in the bias stress effect which decease conductivity. In addition, the W/E voltages are much lower than those typically used in OFETs, and the conductance changes are much faster and more reversible. We attribute the relative ease of polaron formation in the current devices to the reduction of water at a catalytic gate electrode in Au/polythiophene/SiO_2/Pt memory devices, which provide the redox counter-reaction necessary for conductance switching.

5. Conclusions

We have demonstrated an organic memory device based on reversible oxidation and reduction of polythiophene which operates at voltages below 5 V. Conductivity switching in ONVM is determined by polarons in the channel and the memory retention results from stabilization of polarons by a redox counter-reaction at the gate electrode. Thus the mechanism of operation of ONVM is distinctly different from those of the existing OFET memory devices, such as CtFET and FgFET memory devices as these devices depend on charge storage in the electrets layer or the metal nanoparticles. Furthermore, in contrast to several existing OFET memory devices where the mechanism of operation has not been independently confirmed, the mechanism of operation of ONVM has been directly correlated to the polaron concentrations using in situ Raman spectroscopy. With the main components of the redox-based ONVM identified and the ability to spectroscopically monitor memory dynamics, it should be possible to vary the composition and structure to optimize speed, retention, and cycle life.

Acknowledgements

This work was supported by the National Research Council of Canada, the Natural Science and Engineering Research Council of Canada, the National Institute for Nanotechnology, and the University of Alberta. Partial support from a joint project between Xerox Research Centre of Canada and NINT funded by the Nanoworks and NanoAlberta programs of the Province of Alberta is also acknowledged. The Authors thanks Dr. Adam J. Bergren for his help in electrical measurements, Bryan Szeto for mask fabrication, and the Chemistry Machine shop for fabricating masks and accessories for in situ spectroscopic studies.

Appendix A. Supplementary data

Supplementary data associated with this article can be found, in the online version, at http://dx.doi.org/10.1016/j.electacta.2012.11.111.

References

[1] C.Y. Lu, K.Y. Hsieh, R. Liu, Future challenges of flash memory technologies, Microelectronic Engineering 86 (2009) 283.
[2] R. Waser, M. Aono, Nanoionics-based resistive switching memories, Nature Materials 6 (2007) 833.
[3] R. Waser, R. Dittmann, G. Staikov, K. Szot, Redox-based resistive switching memories - nanoionic mechanisms, prospects, and challenges, Advanced Materials 21 (2009) 2632.
[4] J.C. Scott, L.D. Bozano, Nonvolatile memory elements based on organic materials, Advanced Materials 19 (2007) 1452.
[5] Q.D. Ling, D.J. Liaw, C.X. Zhu, D.S.H. Chan, E.T. Kang, K.G. Neoh, Polymer electronic memories: materials, devices and mechanisms, Progress in Polymer Science 33 (2008) 917.
[6] P. Heremans, G.H. Gelinck, R. Muller, K.J. Baeg, D.Y. Kim, Y.Y. Noh, Polymer and organic nonvolatile memory devices, Chemistry of Materials 23 (2011) 341.
[7] J. Lee, E. Lee, S. Kim, G.S. Bang, D.A. Shultz, R.D. Schmidt, M.D.E. Forbes, H. Lee, Nitronyl Nitroxide radicals as organic memory elements with both n- and p-type properties, Angewandte Chemie International Edition 50 (2011) 4414.
[8] A. Bandhopadhyay, A.J. Pal, Large conductance switching and binary operation in organic devices: Role of functional groups, Journal of Physical Chemistry B 107 (2003) 2531.
[9] C.-L. Liu, W.-C. Chen, Donor-acceptor polymers for advanced memory device applications, Polymer Chemistry 2 (2011) 2169.
[10] J.E. Green, J.W. Choi, A. Boukai, Y. Bunimovich, E. Johnston-Halperin, E. Delonno, Y. Luo, B.A. Sheriff, K. Xu, Y.S. Shin, H.R. Tseng, J.F. Stoddart, J.R. Heath, A 160-kilobit molecular electronic memory patterned at 10(11) bits per square centimetre, Nature 445 (2007) 414.
[11] S. Ssenyange, H.J. Yan, R.L. McCreery, Redox-driven conductance switching via filament formation and dissolution in carbon/molecule/TiO_2/Ag molecular electronic junctions, Langmuir 22 (2006) 10689.
[12] N. Knorr, R. Wirtz, S. Rosselli, G. Nelles, Field-absorbed water induced electrochemical processes in organic thin film junctions, Journal of Physical Chemistry C 114 (2010) 15791.
[13] S.M. Wu, T. Tsuruoka, K. Terabe, T. Hasegawa, J.P. Hill, K. Ariga, M. Aono, A polymer-electrolyte-based atomic switch, Advanced Functional Materials 21 (2011) 93.
[14] Y.J. Park, I.S. Bae, S.J. Kang, J. Chang, C. Park, Control of thin ferroelectric polymer films for non-volatile memory applications, IEEE Transactions on Dielectrics and Electrical Insulation 17 (2010) 1135.
[15] K. Asadi, D.M. De Leeuw, B. De Boer, P.W.M. Blom, Organic non-volatile memories from ferroelectric phase-separated blends, Nature Materials 7 (2008) 547.
[16] J.Y. Ouyang, C.W. Chu, C.R. Szmanda, L.P. Ma, Y. Yang, Programmable polymer thin film and non-volatile memory device, Nature Materials 3 (2004) 918.
[17] D. Prime, S. Paul, Overview of organic memory devices INTRODUCTION, Philosophical Transactions of the Royal Society A: Mathematical Physical and Engineering Sciences 367 (2009) 4141.
[18] J. Billen, S. Steudel, R. Muller, J. Genoe, P. Heremans, A comprehensive model for bipolar electrical switching of CuTCNQ memories, Applied Physics Letters 91 (2007) 263507.
[19] F.L.E. Jakobsson, X. Crispin, M. Colle, M. Buchel, D.M. de Leeuw, M. Berggren, On the switching mechanism in Rose Bengal-based memory devices, Organic Electronics 8 (2007) 559.
[20] W.L. Kwan, B. Lei, Y. Shao, Y. Yang, Understanding the switching mechanism of polymer memory, Current Applied Physics 10 (2010) E50.
[21] R. Schroeder, L.A. Majewski, M. Grell, All-organic permanent memory transistor using an amorphous, spin-cast ferroelectric-like gate insulator, Advanced Materials 16 (2004) 633.
[22] R.C.G. Naber, K. Asadi, P.W.M. Blom, D.M. de Leeuw, B. de Boer, Organic nonvolatile memory devices based on ferroelectricity, Advanced Materials 22 (2010) 933.
[23] G.H. Gelinck, A.W. Marsman, F.J. Touwslager, S. Setayesh, D.M. de Leeuw, R.C.G. Naber, P.W.M. Blom, All-polymer ferroelectric transistors, Applied Physics Letters 87 (2005) 092903.
[24] H.E. Katz, X.M. Hong, A. Dodabalapur, R. Sarpeshkar, Organic field-effect transistors with polarizable gate insulators, Journal of Applied Physics 91 (2002) 1572.
[25] K.-J. Baeg, Y.-Y. Noh, J. Ghim, B. Lim, D.-Y. Kim, Polarity effects of polymer gate electrets on non-volatile organic field-effect transistor memory, Advanced Functional Materials 18 (2008) 3678.
[26] W.L. Leong, N. Mathews, B. Tan, S. Vaidyanathan, F. Doetz, S. Mhaisalkar, Towards printable organic thin film transistor based flash memory devices, Journal of Materials Chemistry 21 (2011) 5203.
[27] K.J. Baeg, Y.Y. Noh, J. Ghim, S.J. Kang, H. Lee, D.Y. Kim, Organic non-volatile memory based on pentacene field-effect transistors using a polymeric gate electret, Advanced Materials 18 (2006) 3179.
[28] M. Burkhardt, A. Jedaa, M. Novak, A. Ebel, K. Voitchovsky, F. Stellacci, A. Hirsch, M. Halik, Concept of a molecular charge storage dielectric layer for organic thin-film memory transistors, Advanced Materials 22 (2010) 2525.
[29] J.S. Lee, Recent progress in gold nanoparticle-based non-volatile memory devices, Gold Bulletin 43 (2010) 189.
[30] T. Sekitani, T. Yokota, U. Zschieschang, H. Klauk, S. Bauer, K. Takeuchi, M. Takamiya, T. Sakurai, T. Someya, Organic nonvolatile memory transistors for flexible sensor arrays, Science 326 (2009) 1516.
[31] S.G.J. Mathijssen, M.-J. Spijkman, A.-M. Andringa, P.A. van Hal, I. McCulloch, M. Kemerink, R.A.J. Janssen, D.M. de Leeuw, Revealing buried interfaces to understand the origins of threshold voltage shifts in organic field-effect transistors, Advanced Materials 22 (2010) 5105.
[32] P.A. Bobbert, A. Sharma, S.G.J. Mathijssen, M. Kemerink, D.M. de Leeuw, Operational stability of organic field-effect transistors, Advanced Materials 24 (2012) 1146.
[33] A. Sharma, S.G.J. Mathijssen, M. Kemerink, D.M. de Leeuw, P.A. Bobbert, Proton migration mechanism for the instability of organic field-effect transistors, Applied Physics Letters 95 (2009) 253305.
[34] A.P. Bonifas, R.L. McCreery, In-situ optical absorbance spectroscopy of molecular layers in carbon based molecular electronic devices, Chemistry of Materials 20 (2008) 3849.
[35] A.M. Nowak, R.L. McCreery, In situ Raman spectroscopy of bias-induced structural changes in nitroazobenzene molecular electronic junctions, Journal of the American Chemical Society 126 (2004) 16621.

[36] J. Wu, R.L. McCreery, Solid-State Electrochemistry in Molecule/TiO(2) Molecular Heterojunctions as the Basis of the TiO(2) "Memristor", Journal of the Electrochemical Society 156 (2009) P29.
[37] J. Wu, K. Mobley, R.L. McCreery, Electronic characteristics of fluorene/TiO_2 molecular heterojunctions, Journal of Chemical Physics 126 (2007) 024704.
[38] R.L. McCreery, Analytical challenges in molecular electronics, Analytical Chemistry 78 (2006) 3490.
[39] L.C.T. Shoute, N. Pekas, Y.L. Wu, R.L. McCreery, Redox driven conductance changes for resistive memory, Applied Physics A: Materials Science & Processing 102 (2011) 841.
[40] S. Barman, F.J. Deng, R.L. McCreery, Conducting polymer memory devices based on dynamic doping, Journal of the American Chemical Society 130 (2008) 11073.
[41] A.P. Bonifas, R.L. McCreery, Solid state spectroelectrochemistry of redox reactions in polypyrrole/oxide molecular heterojunctions, Analytical Chemistry 84 (2012) 2459.
[42] B.S. Ong, Y.L. Wu, P. Liu, S. Gardner, High-performance semiconducting polythiophenes for organic thin-film transistors, Journal of the American Chemical Society 126 (2004) 3378.
[43] Y.O. Wu, P. Liu, B.S. Ong, T. Srikumar, N. Zhao, G. Botton, S.P. Zhu, Controlled orientation of liquid-crystalline polythiophene semiconductors for high-performance organic thin-film transistors, Applied Physics Letters 86 (2005) 142102.
[44] A.A. Gewirth, M.S. Thorum, Electroreduction of dioxygen for fuel-cell applications: materials and challenges, Inorganic Chemistry 49 (2010) 3557.
[45] J.-M. Saveant, Molecular catalysis of electrochemical reactions. Mechanistic aspects, Chemical Reviews 108 (2008) 2348.
[46] E. Yeager, Electrocatalysts For O-2 Reduction, Electrochimica Acta 29 (1984) 1527.
[47] R. Kumar, R.G. Pillai, N. Pekas, Y. Wu, R.L. McCreery, Spatially resolved raman spectroelectrochemistry of solid-state polythiophene/viologen memory devices, Journal of the American Chemical Society 134 (2012) 14869.
[48] M. Tello, M. Chiesa, C.M. Duffy, H. Sirringhaus, Charge trapping in intergrain regions of pentacene thin film transistors, Advanced Functional Materials 18 (2008) 3907.
[49] T. Hallam, M. Lee, N. Zhao, I. Nandhakumar, M. Kemerink, M. Heeney, I. McCulloch, H. Sirringhaus, Local charge trapping in conjugated polymers resolved by scanning kelvin probe microscopy, Physical Review Letters 103 (2009) 256803.
[50] R.A. Street, M.L. Chabinyc, F. Endicott, B. Ong, Extended time bias stress effects in polymer transistors, Journal of Applied Physics 100 (2006) 114518.
[51] T. Richards, H. Sirringhaus, Bias-stress induced contact and channel degradation in staggered and coplanar organic field-effect transistors, Applied Physics Letters 92 (2008) 023512.
[52] J.B. Chang, V. Subramanian, Effect of active layer thickness on bias stress effect in pentacene thin-film transistors, Applied Physics Letters 88 (2006) 233513.
[53] R.A. Street, A. Salleo, M.L. Chabinyc, Bipolaron mechanism for bias-stress effects in polymer transistors, Physical Review B 68 (2003) 085316.